Unification of Airy structure in inelastic $\alpha + {}^{16}$O scattering and α-cluster structure with core excitation in ^{20}Ne

Y. Hirabayashi[1] and S. Ohkubo[2,3,*]

[1]*Information Initiative Center, Hokkaido University, Sapporo 060-0811, Japan*
[2]*Research Center for Nuclear Physics, Osaka University, Ibaraki, Osaka 567-0047, Japan*
[3]*University of Kochi, 5-15 Eikokuji-cho, Kochi 780-8515, Japan*

The Airy structure of the nuclear rainbow and prerainbow in inelastic and elastic $\alpha + {}^{16}$O scattering is studied with the coupled channel method using a folding potential derived from the microscopic wave functions of ^{16}O. The theoretical calculations reproduce the characteristic energy evolution of the Airy minimum of the experimental angular distributions. The energy levels with α-cluster structure in ^{20}Ne are reproduced well using the potentials determined from the analysis of scattering. It is shown that the emergence of the $K = 0_3^+$ α-cluster band with core excitation at 7.19 MeV in ^{20}Ne is intimately related to the emergence of the prerainbow and rainbow in inelastic scattering to the ^{16}O(0_2^+). It is found that the α-cluster states with core excitation, the prerainbow and the rainbow in inelastic scattering are understood in a unified way as well as in the case of elastic scattering.

I. INTRODUCTION

Alpha-cluster structure exists widely and essential for understanding nuclear properties in light and medium-weight nuclei [1–4]. The typical ^{20}Ne nucleus with two protons and two neutrons on top of the inert double magic closed shell nucleus ^{16}O has an $\alpha + {}^{16}$O cluster structure and has been studied thoroughly with a cluster model [1–4]. In understanding the α-cluster structure of nuclei the interaction potential between the α particle and the nucleus is very important [4]. The nuclear rainbow can be observed when the absorption is weak or incomplete and the systematic study of nuclear rainbow scattering makes it possible to determine the interaction potential up to the internal region [5].

The elastic α particle scattering from ^{16}O has been studied over a wide range of incident energies theoretically and experimentally [4] and it has been shown that the global optical potential can describe rainbow scattering, prerainbows, anomalous large angle scattering (ALAS) in the low energy region, and the $\alpha + {}^{16}$O cluster structure of ^{20}Ne in a unified way [4,6–8]. The characteristic evolution of the angular distribution from the low energy region where α-cluster structure is relevant to the high energy region where the typical nuclear rainbow appears can be understood very well systematically. The *raison d'etre* of the α-cluster structure in the ground state of ^{20}Ne is thus found to be closely related to the existence of the nuclear rainbows for the $\alpha + {}^{16}$O system. The emergence of the $\alpha + {}^{16}$O structure in the ground state of ^{20}Ne is a consequence of the interaction potential which causes the nuclear rainbow for the $\alpha + {}^{16}$O system. This unified understanding was also successfully applied to the nuclear rainbow in elastic α particle scattering from ^{40}Ca and the α-cluster structure of ^{44}Ti [4,9].

Compared with elastic rainbow scattering, inelastic rainbow scattering has not been studied extensively over a wide range of incident energies both experimentally and theoretically. However, similar to the rainbow in elastic scattering, the study of the inelastic rainbow scattering will be very useful in understanding the interaction potential for the inelastic channels [5,10–13]. The mechanism of the nuclear rainbow and the Airy structure in inelastic scattering has been studied for the $\alpha + {}^{40}$Ca and ^{6}Li + ^{12}C systems by using a phenomenological form factor [14,15]. On the other hand, from the viewpoint of a nuclear structure study it has recently been shown that inelastic nuclear rainbow scattering is powerful in understanding the α-cluster structure of the excited states of the nucleus. For example, the α particle condensate states in ^{12}C and ^{16}O have been revealed by studying the rainbow and prerainbow in α particle and ^{3}He scattering from ^{12}C [16–19]. However, a unified study of inelastic rainbow scattering and α-cluster structure has never been undertaken for the typical $\alpha + {}^{16}$O system.

The purpose of this paper is to understand the nuclear rainbow and prerainbow in inelastic $\alpha + {}^{16}$O scattering, and the α-cluster structure in ^{20}Ne in a unified way. It is shown that the emergence of α-cluster structure with core excitation in ^{20}Ne is closely related to the appearance of Airy structure in the prerainbow and rainbow inelastic α particle scattering from ^{16}O.

II. DOUBLE FOLDING MODEL

We study the elastic and inelastic angular distributions of $\alpha + {}^{16}$O scattering systematically with the coupled channel method using a microscopic double folding model. In the coupled channel calculations we simultaneously take into account the 0_1^+ (0.0 MeV), 0_2^+ (6.05 MeV), 3^- (6.13 MeV), and 2^+ (6.92 MeV) states of ^{16}O. The double folding (DF) potential is constructed from the transition densities of ^{16}O

*ohkubo@yukawa.kyoto-u.ac.jp

using a density-dependent effective interaction:

$$V_{ij}(\mathbf{R}) = \int \rho_{00}^{(\alpha)}(\mathbf{r}_1) \, \rho_{ij}^{(^{16}\mathrm{O})}(\mathbf{r}_2)$$
$$\times v_{NN}(E, \rho, \mathbf{r}_1 + \mathbf{R} - \mathbf{r}_2) \, d\mathbf{r}_1 d\mathbf{r}_2, \qquad (1)$$

where $\rho_{00}^{(\alpha)}(\mathbf{r})$ is the ground state density of the α particle, while v_{NN} denotes the density dependent M3Y effective interaction (DDM3Y) [20] usually used in the DF model. $\rho_{ij}^{(^{16}\mathrm{O})}(\mathbf{r})$ represents the diagonal ($i = j$) or transition ($i \neq j$) nucleon density of ^{16}O which is obtained from the microscopic wave functions calculated in the $\alpha + {}^{12}$C cluster model using the orthogonality condition model (OCM) [21]. The OCM wave functions we take here have been configured by using a realistic size for the α particle and ^{12}C. As a result the agreement of the theoretical calculation with the experiment is further improved from the original $\alpha + {}^{12}$C cluster model wave functions by Suzuki [22], which already excellently reproduced almost all the energy levels of ^{16}O up to $E_x \approx 13$ MeV. This cluster model simultaneously reproduces not only the α-cluster states like the $K = 0^+$ band starting from the mysterious 0^+ state at 6.05 MeV, but also the shell-model-like states such as the 3^- (6.13 MeV) state and the ground state. In the calculations we introduce the normalization factor N_R for the real part of the DF potential [23–25]. We take into account the important transition densities available in Ref. [21], i.e., g.s. $\leftrightarrow 0_2^+$ (6.05 MeV), 3^- (6.13 MeV), 2^+ (6.92 MeV), and 0_2^+ (6.05 MeV) $\leftrightarrow 2^+$ (6.92 MeV) in addition to all the diagonal

couplings. The effect of absorption due to couplings to the other channels is introduced as a phenomenological imaginary potential with a volume-type Woods-Saxon form factor. In previous papers [16–19] this method was successfully applied to the rainbow and prerainbow scattering of α particles and ^{3}He from ^{12}C, where realistic wave functions of ^{12}C calculated in the microscopic α-cluster model were used.

III. AIRY STRUCTURE IN ELASTIC AND INELASTIC $\alpha + {}^{16}$O SCATTERING

We analyze the angular distributions of elastic and inelastic α particle scattering from ^{16}O. Although there are many experimental data available for elastic scattering, experimental angular distributions for inelastic prerainbow and rainbow scattering are only available at the limited energies, 40.5 MeV [26], 50 MeV, 80.7 MeV [27], and 146 MeV [28]. In Fig. 1 the calculated angular distributions are displayed in comparison with the experimental data. The agreement with experimental data, which shows a characteristic energy evolution, is very good. Here the normalization factor for the real part of the potential is slightly adjusted to take account of the energy dependence of the N_R [23–25]. The real potential which reproduces the Airy minimum of rainbow scattering at the highest incident energy 146 MeV is uniquely determined without discrete ambiguity and the obtained volume integral per nucleon pair for elastic channel is 304 MeV fm^3. The
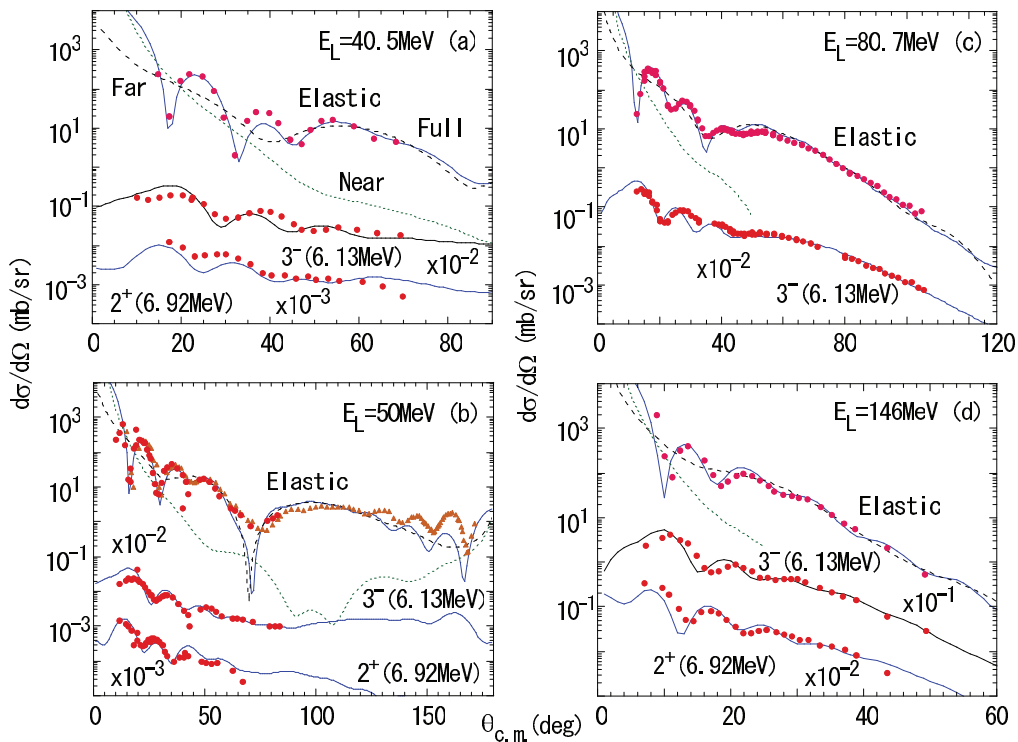

FIG. 1. (Color online) The elastic and inelastic angular distributions (solid lines) of α scattering from ^{16}O calculated using the coupled channel method are compared with the experimental data (red points) at $E_L = 40.5$ MeV [26], 50 MeV, 80.7 MeV [27], and 146 MeV [28]. In (b) the elastic scattering angular distribution calculated at 48.7 MeV is displayed to be compared with the data (orange triangles) measured up to very large angles at 48.7 MeV [8]. The calculated cross sections for elastic scattering (solid lines) are shown decomposed into the farside component (dashed lines) and the nearside component (dotted lines).

TABLE I. The volume integral per nucleon pair J_V, normalization factor N_R, root mean square radius $\langle R^2 \rangle^{1/2}$ of the folding potential, and the parameters of the imaginary potentials in the conventional notation.

E_L (MeV)	N_R	J^π	J_V (MeV fm^3)	$\langle R^2 \rangle^{1/2}$ (fm)	W_V (MeV)	R_V (fm)	a_V (fm)
40.5	1.42	0_1^+	395	3.61	5.0	5.1	0.5
		0_2^+	425	3.77	5.0	5.1	0.5
		3^-	394	3.58	5.0	5.1	0.5
		2^+	429	3.79	8.0	5.1	0.5
50	1.42	0_1^+	390	3.61	5.5	5.1	0.3
		0_2^+	418	3.77	6.0	5.1	0.3
		3^-	388	3.58	6.0	5.1	0.3
		2^+	422	3.79	11.0	5.1	0.3
80.7	1.34	0_1^+	347	3.62	7.1	5.2	0.4
		0_2^+	373	3.78	10.0	5.2	0.4
		3^-	346	3.59	10.0	5.2	0.4
		2^+	377	3.79	10.0	5.2	0.4
146	1.34	0_1^+	304	3.65	9.0	5.2	0.4
		0_2^+	328	3.80	13.0	5.2	0.4
		3^-	303	3.62	13.0	5.2	0.4
		2^+	331	3.82	12.0	5.2	0.4

N_R values at the lower energies are determined by slightly adjusting to fit the experimental data. The imaginary potential is mostly responsible for reducing the magnitude of the cross sections. In the calculations the strength parameter of the imaginary potential (W_V) was fitted to reproduce the magnitude of the experimental cross sections while the radius parameter and the diffuseness parameter were fixed at around $R_V = 5$ fm and

$a_V = 0.3$–0.5 fm, respectively. These approaches using the folding potential have been shown successful for the α and ^{3}He scattering from ^{12}C [16,17,19] over a wide rage of incident energies. The properties of the real folding potential and potential parameters used in the analysis are given in Table I. The energy dependence of the volume integrals for the elastic channel is physically reasonable and consistent with the phenomenological potentials [7] and the folding model potentials [8,25] obtained in the analysis of elastic α particle scattering from ^{16}O. For elastic scattering the calculated angular distributions are decomposed into farside and nearside components. The angular distributions are dominated by the refractive farside component and the Airy minimum is observed at $\sim 18°$, $\sim 36°$, and $\sim 78°$ for $E_L = 146$ MeV, 80.7 MeV, and 48.7 MeV, respectively. For 40.5 MeV, although the experimental data are available only up to $\sim 68°$, the theoretical calculation predicts an Airy minimum at $\sim 85°$.

In Fig. 2 the energy evolution of the Airy structure in the angular distributions for elastic scattering is shown in comparison with that of inelastic scattering to the 0_2^+ state and the 3^- state. As seen in Fig. 2(a) the Airy minimum moves toward large angles as the incident energy decreases from rainbow scattering to prerainbow scattering. This is reasonable considering that the refractive index increases and refraction becomes stronger as the incident energy decreases.

The prerainbow at 40.5 MeV and around 50 MeV develops into the typical rainbow at the higher energies, 80.7 MeV and 146 MeV with the falloff of the cross sections in the angular distribution at the darkside beyond the rainbow angle and with the first order Airy minimum and Airy maximum of the bright side at angles smaller than the rainbow angle. In
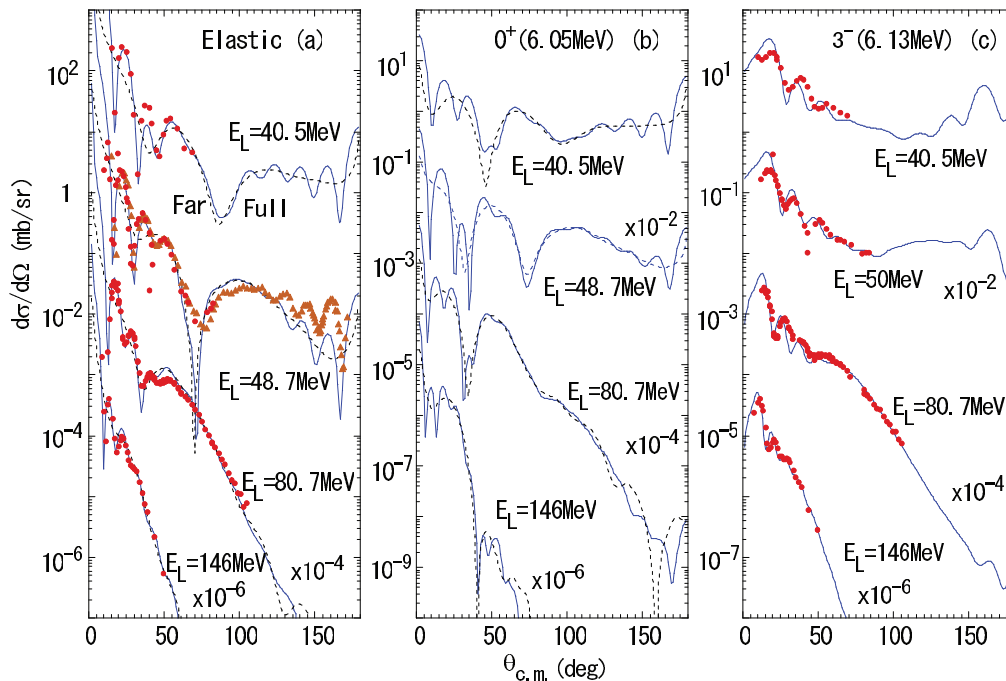

FIG. 2. (Color online) The energy evolution of the Airy minimum in the calculated (solid lines) and experimental (red points and orange triangles) angular distributions of prerainbow and rainbow $\alpha + {}^{16}$O scattering, is displayed for (a) elastic scattering, (b) inelastic scattering to the 0_2^+ state, and (c) inelastic scattering to the 3^- state. The farside cross sections are shown with dashed lines. The experimental data (red points) at 50 MeV are also included for the 48.7 MeV case in (a).
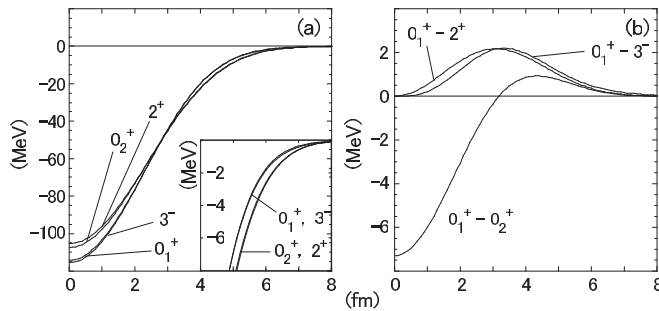
FIG. 3. The double folding diagonal (a) and coupling (b) potentials for the $\alpha + {}^{16}$O system calculated at $E_L = 50$ MeV.

Fig. 2(c) the nuclear rainbow is observed to behave similarly in inelastic scattering to the 3^- (6.13 MeV) state at 80.7 and 146 MeV, which shows that the absorption is not strong for inelastic scattering. This suggests that the inelastic rainbow scattering can serve to determine the interaction potential for inelastic scattering and the transition form factors including the internal region. The very good agreement of the theoretical calculations with the experimental data shows that the present potential for the inelastic channel derived from the OCM microscopic cluster wave functions is reliable up to the internal region. The Airy minimum for the rainbow scattering to the 3^- state is observed at $\sim 27°$ and $\sim 44°$ for 146 MeV and 80.7 MeV, respectively. The fall-off of the angular distribution characteristic to the rainbow at the high energy region is seen at 146 MeV and 80.7 MeV for the inelastic scattering to the 3^- state and the Airy minimum of the indication of the prerainbow is seen at around $88°$ in the 50 MeV angular distribution, although the experimental data are available only up to $83°$.

The good agreement of the calculated angular distributions with the experimental data in Fig. 1 shows that the interaction potentials constructed from the OCM wave function are reliable up to the internal region. This makes it possible to investigate the energy evolution of the Airy minimum for the 0_2^+ (6.05 MeV) state reliably. Although the experimental data

have not been measured, we see in Fig. 2(b) that the evolution of the angular distributions for this state is very similar to that for elastic scattering. It is interesting to note that although the two 0^+ states have a very different structure, shell-like spherical for the ground state and the deformed well-developed α-cluster structure for the 0_2^+ state, the essential behavior of the two angular distributions is similar. With refractive scattering the target nucleus behaves as a lens. The similarity may be related to the fact that the difference in the sizes of the two states is not large: the calculated rms radius of the matter density distribution is 2.58 fm for the ground state and 2.77 fm for the 0_2^+ state.

In Fig. 3 the diagonal and coupling interaction potentials are displayed. The diagonal potential for the 3^- state is similar to that for the ground state in magnitude and shape. We see in Table I that the volume integrals and rms radii of the potentials for the ground state and the 3^- state are very similar. These two states have a compact shell-model structure. On the other hand, the diagonal potentials for the 0_2^+ and 2^+ states are significantly shallower in the internal region and deeper in the surface region compared with those for the ground and 3^- states. This is due to the fact that the 0_2^+ and 2^+ states have a well-developed $\alpha + {}^{12}$C cluster structure. However, this difference of the interaction potential is important when we want to understand the bound and quasibound states of the $\alpha + {}^{16}$O system, the low energy prerainbow scattering and the high-energy rainbow scattering in an inelastic channel in a unified way, although in phenomenological studies the same potential is often used for elastic and inelastic channels. It is also important to point out that the form factor of the coupling from the ground state to the 0_2^+ state has a node and is different from a phenomenological monopole vibrational form factor derived from the Woods-Saxon potential.

In Fig. 4 the energy evolution of the farside component of the calculated angular distributions for elastic scattering and inelastic scattering to the 0_2^+ state is compared in 4 MeV steps. The energy dependence of N_R and parameters of the imaginary potentials in-between is interpolated from those which fit the
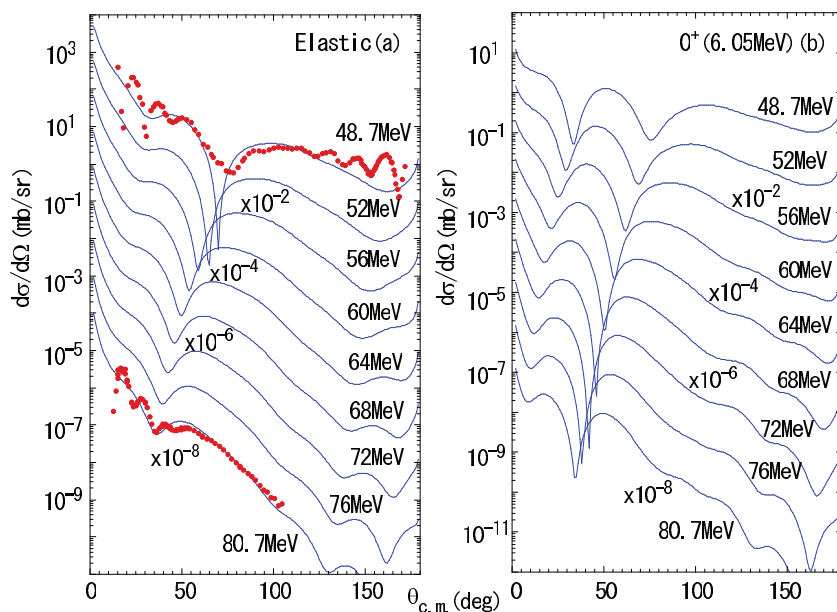

FIG. 4. (Color online) The energy evolution of the farside component of the angular distributions calculated in 4 MeV steps for (a) elastic scattering and (b) inelastic scattering to the 0_2^+ state (solid lines) and the experimental data (points) [8,27].
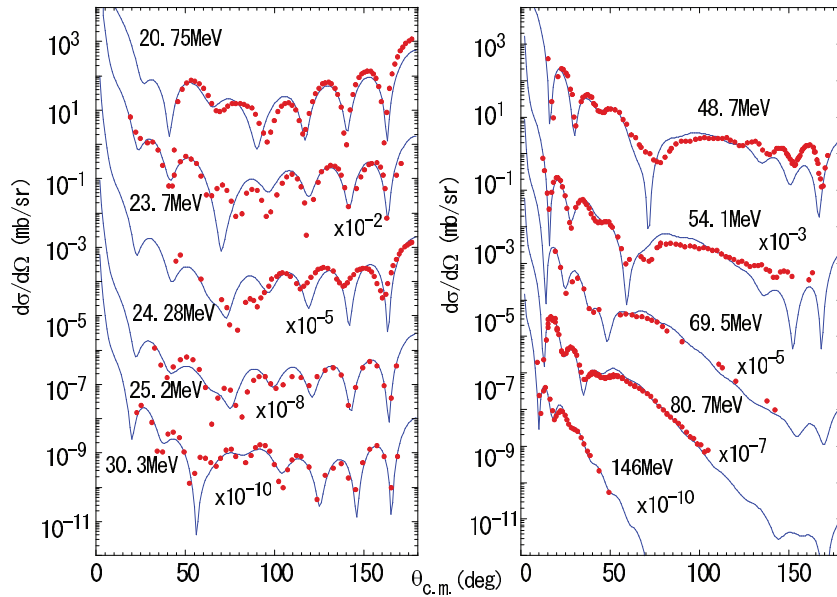
FIG. 5. (Color online) The energy evolution of the angular distributions in elastic $\alpha + {}^{16}\text{O}$ scattering calculated using the coupled channel method (solid lines) is displayed in comparison with the experimental data (points), 20.7 MeV [29], 23.7 MeV [30], 24.28 MeV [29], 25.2 MeV [31], 30.3 MeV [31], 48.7 MeV, 54.1 MeV [8], 69.5 MeV [7], 50 MeV, 80.7 MeV [27], and 146 MeV [28].

experimental angular distributions at 48.7 MeV and 80.7 MeV. The evolution of the Airy minimum, which shifts to forward angles as the incident energy increases, is clearly seen. In the inelastic scattering the second order Airy minimum is seen. The similarity of the evolution between the elastic scattering and the inelastic scattering to the 0_2^+ state persists from the lowest energy to the highest energy. This similarity also persists to the lower energy ALAS region. Although no experimental data for the 0_2^+ state are available, angular distributions similar to the elastic scattering, if measured, are expected. The observation will be very useful for clarifying the coupling form factor between the two 0^+ states with a very different structure experimentally.

IV. α-CLUSTER STRUCTURE IN ^{20}Ne

In Fig. 5 we show that the present folding potentials using the microscopic wave functions can reproduce the elastic scattering up to the low energy region where ALAS appears systematically. The imaginary potential simply takes into account the reduction of the flux due to absorption and the essential structure of the angular distributions is characterized by the real part of the optical potential. The N_R values used are reasonably consistent with Table I and are 1.42, 1.38, 1.42, 1.42, 1.36, 1.32, 1.36, and 1.42 for 69.5 MeV, 54.1 MeV, 48.7 MeV, 30.3 MeV, 25.2 MeV, 24.28 MeV, 23.7 MeV, and 20.75 MeV, respectively. The pronounced oscillation of the angular distributions at the backward angles at $20 \sim 25$ MeV is due to the highly excited $\alpha + {}^{16}\text{O}$ cluster structure in ^{20}Ne [6,7]. This suggests the present potential is useful even for the much lower energy region including the bound energy region. In fact, the lowest Pauli allowed states that the real potential for the elastic channel accommodate satisfy the Wildermuth condition $2n + L = 8$ where n is the number of the nodes and L is the orbital angular momentum of the relative wave function and correspond to the $K = 0_1^+$ band of ^{20}Ne (Fig. 6) with the $\alpha + {}^{16}\text{O}$ cluster structure.

In Figs. 6(b) and 6(d) the energy levels of ^{20}Ne calculated in the bound state approximation using the diagonal potentials with $N_R = 1.245$ for the elastic and the 0_2^+ channels, respectively, are shown in comparison with the experimental levels. The N_R used is the one adjusted to reproduce the experimental binding energy of the ground state of ^{20}Ne, 4.73 MeV, from the α threshold. The calculation reproduces the experimental energy levels of the $K = 0_1^+$ ground band, its parity doublet partner $K = 0^-$ band and the higher nodal $K = 0_4^+$ band with the $\alpha + {}^{16}\text{O(g.s.)}$ cluster structure well. In Fig. 6(d) we see that the calculated lowest 0^+ state with the $\alpha + {}^{16}\text{O}(0_2^+)$ structure corresponds well to the experimental $K = 0_3^+$ band starting at $E_x = 7.19$ MeV [Fig. 6(c)] with the ${}^{12}\text{C} + \alpha + \alpha$ cluster [2]. The agreement with the experimental $K = 0_3^+$ band will be improved by taking into account the coupling between the two
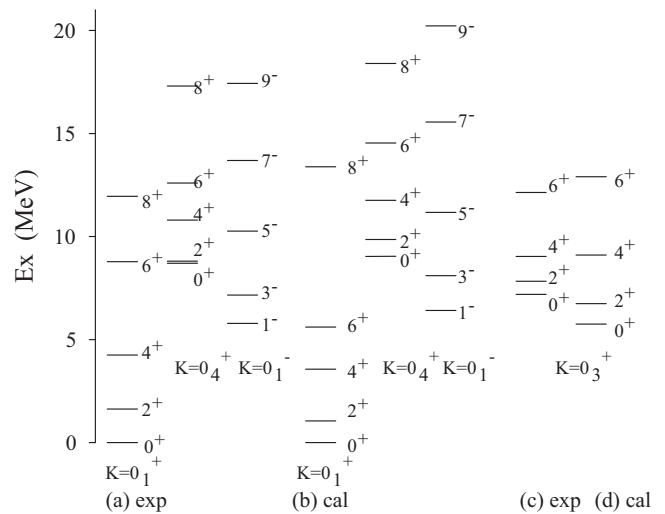

FIG. 6. The experimental $K = 0_1^+$, $K = 0_1^-$, and $K = 0_4^+$ bands with the $\alpha + {}^{16}\text{O(g.s.)}$ structure (a), and the $K = 0_3^+$ band with the $\alpha + {}^{16}\text{O}^*(0_2^+)$ structure (c) are compared with the calculated energy levels with the folding potentials for the $\alpha + {}^{16}\text{O}$ (b) and $\alpha + {}^{16}\text{O}^*(0_2^+)$ (d) channels, respectively.

channels because the calculated 0^+ state with the $\alpha + {}^{16}O(0_2^+)$ structure is pushed higher due to the orthogonality to the ground state. The excitation energy 7.19 MeV of the 0_3^+ in ${}^{20}Ne$ is close to the excitation energy 6.05 MeV of the 0_2^+ state in ${}^{16}O$. In this unified description of the $K = 0_3^+$ band and inelastic scattering it is very important that the potential for the 0_2^+ channel is slightly shallower in the internal region compared with the elastic channel, as shown in Fig. 3. The interaction potential which describes well the inelastic rainbow scattering for the $\alpha + {}^{16}O$ inevitably predicts the existence of an α-cluster structure with core excitation near the threshold energy supporting the Ikeda's threshold rule [2] even for a core-excited cluster case. Thus the emergence of the α-cluster structure with core excitation in the bound state energy region is considered to be in line with the rainbow, prerainbow, and ALAS for the inelastic channel as in the case for the elastic channel.

V. SUMMARY AND CONCLUSIONS

To summarize, we analyzed the nuclear rainbow, prerainbow and ALAS in inelastic scattering of α particles from ${}^{16}O$ as well as elastic scattering in the coupled channel method by using a double folding potential derived from microscopic cluster wave functions. The calculations reproduce the experimental angular distributions well over a wide range of incident energies and can explain the energy evolution of the Airy minimum in the ALAS, prerainbow and rainbow systematically. The theoretical calculations predict a clear nuclear rainbow and prerainbow in inelastic α particle

scattering to the 0_2^+ (6.05 MeV) state of ${}^{16}O$ that resembles the elastic scattering. The interaction potential for the inelastic channel can be well determined from the analysis of inelastic nuclear rainbow scattering as was the case for the elastic scattering. This indicates that the interaction potential for the inelastic channel can also describe the α-cluster state of ${}^{20}Ne$ with the ${}^{12}C + \alpha$ core excitation. Our potential locates the $K = 0_3^+$ α-cluster band with core excitation in ${}^{20}Ne$ in good agreement with experiment in addition to the $K = 0_1^+$, $K = 0_1^-$ and $K = 0_4^+$ bands with the $\alpha + {}^{16}O(g.s.)$ structure. In conclusion, we have shown for the first time that the α-cluster structure with core excitation, the ALAS, the prerainbow and the nuclear rainbow with its beautiful energy evolution of the Airy structure can be understood in a unified way. Inelastic nuclear rainbow scattering is useful not only for extracting the interaction potential but also for the understanding of the α-cluster structure with core excitation in the bound state region.

[1] R. Tamagaki *et al.*, Prog. Theor. Phys. Suppl. **52**, 1 (1972), and references therein.

[2] K. Ikeda *et al.*, Prog. Theor. Phys. Suppl. **68**, 1 (1980), and references therein.

[3] S. Ohkubo, M. Fujiwara, and P. E. Hodgson, Prog. Theor. Phys. Suppl. **132**, 1 (1998) and references therein.

[4] F. Michel, S. Ohkubo, and G. Reidemeister, Prog. Theor. Phys. Suppl. **132**, 7 (1998) and references therein.

[5] D. T. Khoa, W. von Oertzen, H. G. Bohlen, and S. Ohkubo, J. Phys. G **34**, R111 (2007).

[6] S. Ohkubo, Y. Kondo, and S. Nagata, Prog. Theor. Phys. **57**, 82 (1977).

[7] F. Michel, J. Albinski, P. Belery, T. Delbar, G. Gregoire, B. Tasiaux, and G. Reidemeister, Phys. Rev. C **28**, 1904 (1983).

[8] H. Abele and G. Staudt, Phys. Rev. C **47**, 742 (1993).

[9] F. Michel, G. Reidemeister, and S. Ohkubo, Phys. Rev. Lett. **57**, 1215 (1986).

[10] H. G. Bohlen, M. R. Clover, G. Ingold, H. Lettau, and W. von Oertzen, Z. Phys. A **308**, 121 (1982).

[11] H. G. Bohlen *et al.*, Z. Phys. A **322**, 241 (1985).

[12] H. G. Bohlen *et al.*, Z. Phys. A **346**, 189 (1993).

[13] D. T. Khoa *et al.*, Nucl. Phys. A **759**, 3 (2005).

[14] F. Michel and S. Ohkubo, Phys. Rev. C **70**, 044609 (2004); Nucl. Phys. A **738**, 231 (2004).

[15] F. Michel and S. Ohkubo, Phys. Rev. C **72**, 054601 (2005).

[16] S. Ohkubo and Y. Hirabayashi, Phys. Rev. C **70**, 041602(R) (2004).

[17] S. Ohkubo and Y. Hirabayashi, Phys. Rev. C **75**, 044609 (2007).

[18] S. Ohkubo and Y. Hirabayashi, Phys. Lett. B **684**, 127 (2010).

[19] Sh. Hamada, Y. Hirabayashi, N. Burtebayev, and S. Ohkubo, Phys. Rev. C **87**, 024311 (2013).

[20] A. M. Kobos, B. A. Brown, R. Lindsaym, and G. R. Satchler, Nucl. Phys. A **425**, 205 (1984).

[21] S. Okabe, in *Tours Symposium on Nuclear Physics II*, edited by H. Utsunomiya *et al.* (World Scientific, Singapore, 1995), p. 112.

[22] Y. Suzuki, Prog. Theor. Phys. **55**, 1751 (1976); **56**, 111 (1976).

[23] G. R. Satchler and W. G. Love, Phys. Rep. **55**, 183 (1979).

[24] M. E. Brandan and G. R. Satchler, Phys. Rep. **285**, 143 (1997).

[25] D. T. Khoa, Phys. Rev. C **63**, 034007 (2001).

[26] B. G. Harvey, J. R. Meriwether, J. Mahoney, and A. B. de Nercy, Phys. Rev. **146**, 712 (1966).

[27] M. Reed, UCRL-18414 [1968 (unpublished)].

[28] K. T. Knöpfle, G. J. Wagner, H. Breuer, M. Rogge, and C. Mayer-Böricke, Phys. Rev. Lett. **35**, 779 (1975).

[29] M. Takeda, S. Kato, and T. Yamazaki, J. Phys. Soc. Japan **30**, 56 (1971).

[30] G. A. Feofilov, A. E. Denisov, R. P. Kolalis, and V. S. Sadkovskiy, J. Izv. **40**, 2210 (1976).

[31] A. V. Ignatenko, V. M. Lebedev, N. V. Orlova, and A. V. Spassky, Yad. Fiz. **59**, 597 (1996) [Phys. At. Nucl. **59**, 565 (1996)].